MULTI-OBJECTIVE OPTIMIZATION OF FORMING TIME AND SURFACE ROUGHNESS IN TWO-POINT INCREMENTAL FORMING OF A1050-H14 ALUMINUM USING BOX-BEHNKEN DESIGN AND NSGA-II

Huu-That Nguyen[1], Van-Viet Ma[2,*]

DOI: https://doi.org/10.57001/huih5804.2026.009

ABSTRACT

This study proposes a multi-objective optimization strategy for optimizing forming time (T) and surface roughness (R_a) in the Two-point incremental forming (TPIF) process applied to A1050-H14 aluminum sheets. A Box–Behnken Design was employed to create the experimental matrix, which included four key process parameters: depth step (Δz), feed rate (V_{xy}), spindle speed (n), and tool diameter (D). Experiments were conducted on genuine TPIF systems to acquire empirical data. The statistical analysis findings reveal that Δz was the parameter with the most significant effect on T, whereas D was the parameter with the most significant influence on R_a. Response Surface Methodology (RSM) was used to generate regression models for T and R_a. Subsequently, using the NSGA-II approach, the optimum Pareto solution for the TPIF process of A1050-H14 was created, balancing R_a and T. The best settings, including $\Delta z = 0.78$mm, $V_{xy} = 1137$mm/min, $n = 1577$rpm, and $D = 15.75$mm, produced $R_a = 1.13$µm and $T = 7.26$min. This indicates that achieving high efficiency and good surface quality requires selecting values on the Pareto curve.

Keywords: *Two-point incremental forming, Forming time, Surface roughness, Multi-objective optimization.*

[1]Faculty of Mechanical Engineering, Nha Trang University, Vietnam

[2]Faculty of Mechanical Technology, Ho Chi Minh City University of Industry and Trade (HUIT), Vietnam

[*]Email: vietmv@huit.edu.vn

Received: 05/9/2025

Revised: 08/11/2025

Accepted: 28/01/2026

1. INTRODUCTION

Today, incremental sheet forming (ISF) technology has become an essential solution in industrial manufacturing due to its simplicity and the fact that it eliminates the need for molds. Compared to traditional forming technologies such as stamping, drawing, stretching, and pressing, which rely on molds and dies to create precise products, ISF offers greater flexibility in production [1, 2]. While traditional methods can produce accurate products, they are limited in design diversity and are only suitable for mass production [3]. In contrast, the demand for producing small quantities, diverse designs, and low-cost products is increasingly important in aerospace, automotive, and medical industries [4, 5]. Molding-free technology, particularly ISF, provides the ideal solution to meet these needs by reducing costs and increasing flexibility in producing small- to medium-batch products.

ISF technology has two primary methods: Single Point Incremental Forming (SPIF) and Two Point Incremental Forming (TPIF). SPIF uses a single spherical tool to form a metal sheet layer by layer. This method is low-cost and straightforward, but it cannot create features with concave and convex areas, and its ability to form complex shapes is limited [1]. In contrast, TPIF utilizes two tools in combination with fixed dies, enabling the creation of complex features that include both concave and convex areas. TPIF provides more accurate products with better surface quality than SPIF, allowing the formation of difficult-to-deform materials such as stainless steel and titanium [3].

In the automotive and aerospace industries, A1050-H14 material, a high-strength aluminum alloy with excellent corrosion resistance, is widely used for manufacturing casing components. However, the high ductility of A1050-H14 makes forming difficult with traditional methods, especially for complex components.

As a result, TPIF technology is an ideal choice for machining this material [3, 6]. Recent studies have been conducted to explore the application of TPIF for A1050-H14. For example, many authors analyzed the effects of process parameters on the material's formability and identified defects in the product after forming.

Optimizing process parameters is essential for improving productivity and product quality, reducing production time, and preventing undesirable defects. Although several studies have utilized single-objective optimization methods, such as Taguchi combined with the Grey method [2], or multi-objective optimization methods like PSO [7] or RSM [8], these methods typically only help find optimal values for certain factors. However, the optimal results may not be comprehensive in all cases, especially when real-world conditions change or there is uncertainty in parameters. Furthermore, these methods can lead to increased production costs because they may not achieve a compromise between objectives. In practical manufacturing, optimization often requires trade-offs between output goals, such as between productivity and product quality [9]. Depending on the situation, operators may prioritize improving productivity and accept a moderate quality level to avoid increasing production costs and product prices. Therefore, the NSGA-II multi-objective optimization method provides a more effective solution, allowing operators to prioritize objectives and compromise on other goals, thereby determining the optimal process parameters for production [9].

In this study, the author applies the multi-objective optimization approach to improve T and R_a in the TPIF process applied to A1050-H14 aluminum sheets. A Box-Behnken Design (BBD) was employed to structure the experimental matrix, comprising four key process parameters: depth step (Δz), feed rate (V_{xy}), spindle speed (n), and tool diameter (D). Actual experiments were conducted, and the results were analyzed using the global effect charts to identify significant factors. Response Surface Methodology was used to construct regression models for T and R_a. Finally, the NSGA-II algorithm was applied to optimize, minimize R_a and T. This research demonstrates an integrated statistical-experimental framework for improving both quality and productivity in the TPIF process.

2. MATERIALS AND METHODS

2.1. Experimental material and equipment

The workpiece used in the experiment was an A1050-H14 aluminum sheet with a size of 300 x 300mm^2 and a thickness of 1.5mm. This material is primarily composed of aluminum (Al), with trace amounts of impurities such as iron (Fe), silicon (Si), copper (Cu), zinc (Zn), and titanium (Ti). Aluminum makes up the majority of the composition. The physical properties of an A1050-H14 aluminum sheet include a density of 2.71g/cm^3, a thermal expansion coefficient of $24\times10^{-6}K^{-1}$, a thermal conductivity of 222W/mK, and an electrical resistivity of $0.028210^{-6}\Omega$.m. In terms of mechanical properties, this aluminum sheet has a maximum tensile strength of 145MPa, a minimum yield strength of 85MPa, and an elongation of 16%, making it suitable for various experimental and simulation applications [3]. The workpiece was securely fixed between a movable base plate and a clamping plate, held in place by eight heavy-duty screws to prevent it from slipping during the forming process. The sheet metal part was oriented vertically by four precision guide rails, which were integrated into a custom-designed jig and fixture system, as shown in Figure 1. This system was securely mounted to the work-table of the GSK983M Milling CNC System at DCSELAB (Digital Control and System Engineering Laboratory), Ho Chi Minh City University of Technology, with the following technical specifications: travel along the three axes OX, OY, OZ: X = 800mm, Y = 500mm, Z = 300mm; machine table dimensions 1200 mm x 800 mm; spindle power 4.5kW, speed range from 400 to 4000RPM; stable spindle speed range from 300RPM to 2000RPM, as indicated in Figure 2, ensuring structural rigidity and positional accuracy throughout the forming process [3].

The experiment was conducted using the layer method, employing a roller-ball tool with a diameter D ranging from 6 to 18mm, characterized by very high hardness, and mounted directly on the drive shaft of the CNC forming machine, as illustrated in Figure 3.

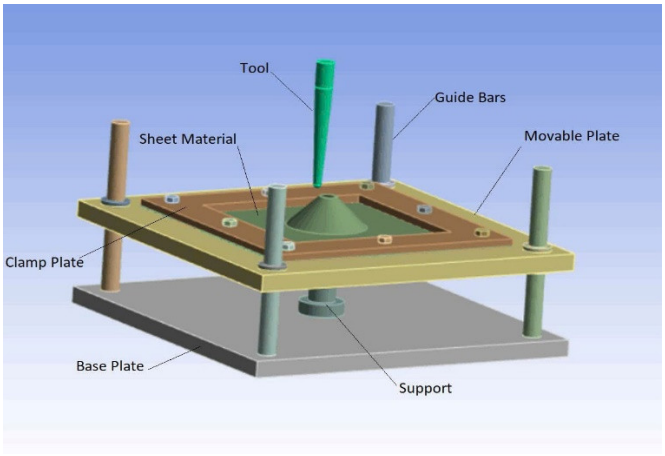

Figure 1. Jig and fixture system

Figure 2. Experiment system for the TPIF process

Figure 3. Tow-point incremental forming tool

Before each tool change for a new experiment, the tool needs to be reset to ensure the dimensional accuracy of the formed product. Friction-reducing lubrication during TPIF is crucial in reducing tool wear, which in turn affects product quality. Therefore, this study employed a lubricant composed of a 1:1 ratio of solid graphite powder and lithium-based grease, combined with multigrade engine oil (SAE 20W-50) [3].

2.2. Experimental design

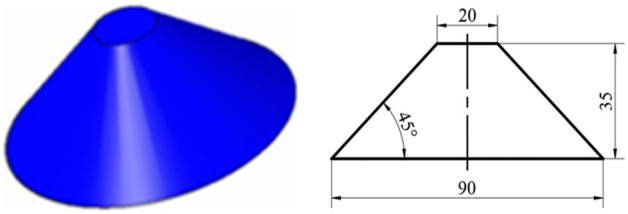

(a) (b)

Figure 4. (a) CAD model of forming product, (b) Geometric profile of forming product

Table 1. Machining parameters for experimental design

No	Machining parameters	Unit	Level		
			1	2	3
1	Depth step (Δz)	mm	0.1	0.8	1.5
2	Feed rate (V_{xy})	mm/min	300	900	1500
3	Spindle speed (n)	rpm	300	1050	1800
4	Tool diameter (D)	mm	6	12	18

In this study, the investigated product model is selected as a truncated cone, as shown in Figure 4. The experimental design method employs the Box-Behnken method, a widely used approach for effectively exploring the parameter space. Four main process parameters, including depth step (Δz), feed rate (V_{xy}), tool diameter (D), and spindle speed (n), are selected based on previous studies, as shown in Table 1. Each parameter is divided into three levels and arranged in 29 experiments as shown in Table 2.

The primary response variables for the analysis are the forming time and the surface roughness of the product. A specialized CNC forming machine directly determines the forming time (T), as shown in Figure 3. After each experiment, the roughness (R_a) of the formed surface is measured by the Surftest SJ-301 by Mitutoyo. Figure 5 depicts the end products obtained from these testing runs, providing a visual picture of the pieces' final shape and surface quality.

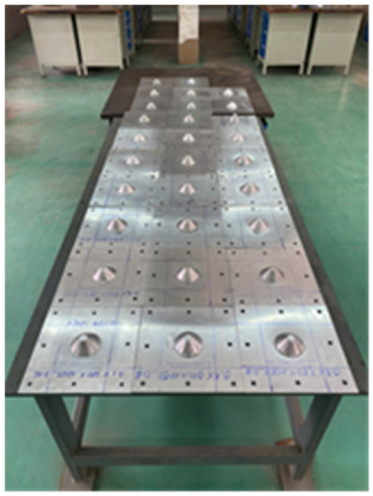

Figure 5. The forming products

Table 2. Design of experiments and results for forming time (T) and surface roughness (R_a)

No	Δz (mm)	V_{xy} (mm/min)	n (rpm)	D (mm)	T (min)	R_a (µm)
1	0.1	300	1050	12	55	2.0
2	1.5	300	1050	12	22	2.0
3	0.1	1500	1050	12	23	1.6
4	1.5	1500	1050	12	18	2.4
5	0.8	900	300	6	32	1.8
6	0.8	900	1800	6	20	2.0
7	0.8	900	300	18	27	0.5
8	0.8	900	1800	18	10	0.4
9	0.1	900	1050	6	48	2.1
10	1.5	900	1050	6	16	2.2
11	0.1	900	1050	18	28	0.4
12	1.5	900	1050	18	19	0.8
13	0.8	300	300	12	48	1.7

14	0.8	1500	300	12	16	2.0
15	0.8	300	1800	12	22	1.9
16	0.8	1500	1800	12	12	1.7
17	0.1	900	300	12	52	1.6
18	1.5	900	300	12	23	1.8
19	0.1	900	1800	12	24	1.7
20	1.5	900	1800	12	15	2.1
21	0.8	300	1050	6	45	2.0
22	0.8	1500	1050	6	18	2.1
23	0.8	300	1050	18	30	0.5
24	0.8	1500	1050	18	10	0.4
25	0.8	900	1050	12	13	1.7
26	0.8	900	1050	12	13	1.7
27	0.8	900	1050	12	13	1.7
28	0.8	900	1050	12	13	1.7
29	0.8	900	1050	12	13	1.8

2.3. Optimization methodology

The NSGA-II is a widely recognized and effective method for addressing multi-objective optimization problems. Multi-objective optimization involves identifying solutions that balance and optimize several conflicting objectives simultaneously. This process typically results in a collection of non-dominated solutions, known as the Pareto front. Given its computational efficiency, the NSGA-II algorithm is applied in this study to tackle the multi-objective optimization problem related to R_a and T in multi-point metal geometry. The process for optimizing R_a and T is illustrated in Figure 6 [10].

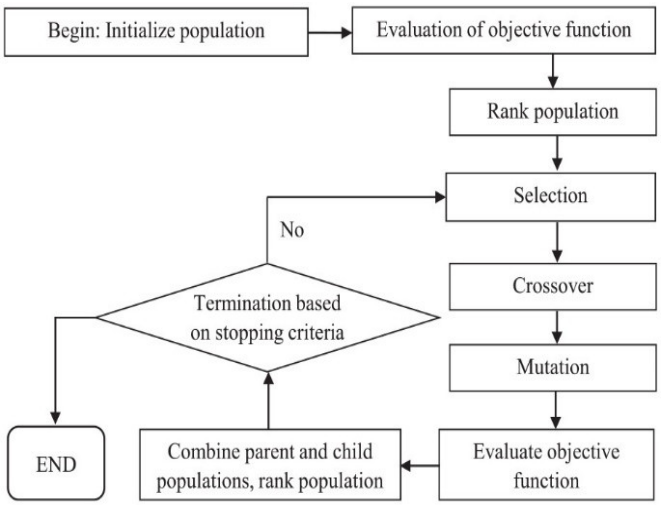

Figure 6. A procedure of the NSGA-II technique for multi-objective optimization in the TPIF

3. RESULTS AND DISCUSSION

3.1. Regression modeling and statistical analysis

After conducting all the pre-established experiments based on the input parameters of the TPIF process, the measured data for R_a and T are presented in Table 2. These results were used to develop a regression model using RSM and to statistically analyze the influence of independent and interacting variables on the output responses, including R_a and T.

According to Table 3, the quadratic empirical regression models were constructed based on the RSM method, describing the interactions between input process parameters and output results for R_a and T during the TPIF process for A1050 H14 aluminum sheet, as shown in Equations (1) and (2).

$$\begin{aligned} T = {} & 164.58 - 88.01\Delta z - 0.08436V_{xy} - 0.04357n \\ & - 5.338D + 20.41\,\Delta z\times\Delta z + 1.944.\,10^{-5}\,V_{xy}\times \\ & V_{xy} + 0.844.\,10^{-5}\,n\times n + 0.1389\,D\times D \\ & + 0.01667\,\Delta z\times V_{xy} + 0.00952\,\Delta z\times n \\ & + 1.369\,\Delta z\times D + 1.222.\,10^{-5}\,V_{xy}\times n \\ & + 0.000486\,V_{xy}\times D - 0.000278\,n\times D \end{aligned} \quad (1)$$

$$\begin{aligned} R_a = {} & 1.246 - 1.028\,\Delta z - 0.000442\,V_{xy} \\ & + 0.000533\,n + 0.2418\,D + 0.3197\,\Delta z\times\Delta z \\ & + 2.963.10^{-7}\,V_{xy}\times V_{xy} - 0.548.10^{-7}\,n\times n \\ & - 0.014745\,D\times D + 4.762.10^{-4}\,\Delta z\times V_{xy} \\ & + 0.952.10^{-4}\,\Delta z\times n + 0.01786\,\Delta z\times D \\ & - 0.2778.10^{-6}\,V_{xy}\times n - 1.39.10^{-5}\,V_{xy}\times D \\ & -1.667.10^{-5}\,n\times D \end{aligned} \quad (2)$$

Furthermore, in statistical analysis, R^2 represents the coefficient of determination, which quantifies the goodness of fit of the regression model to the experimental data. As indicated by the assessment of the RSM models for T and R_a shown in Figure 7, the R^2 values for T and R_a are 0.992 and 0.952, respectively, very close to 1. These results suggest that the models account for over 95% of the total variance. Therefore, they can be considered highly reliable for predicting R_a and T within the range of input variables investigated during the TPIF process.

Figure 8 illustrates the global influence of the investigated parameters on two key indicators, T and R_a, using average gradients. In graph (8-a), it is evident that Delta z (**Δz**) exerts the most substantial effect on T, with an average gradient approaching 0.7. This is followed by the V_{xy} and n, which exhibit average gradients of approximately 0.55 and 0.3, respectively. Conversely, the D has the least impact, with a gradient of less than 0.3. In contrast, graph (8-b) reveals that D has the most

significant influence on R_a, with an average gradient close to 0.9. The remaining parameters have comparatively lower impacts, with average gradients of less than 0.3. This analysis of the global effects of process variables indicates that **Δ***z* and *D* are the two most influential factors on both *T* and R_a when performing the TPIF of A105-H14. These findings align with previous studies in the TPIF process, which have consistently demonstrated that **Δ**z and *D* play critical roles in determining the quality of the formed product [11].

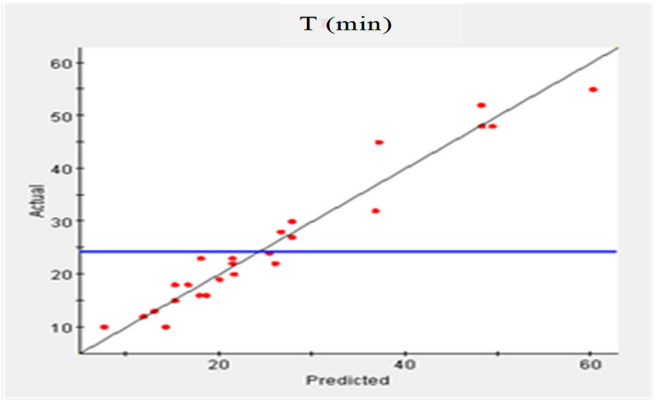

(a) $R^2 = 0.992$

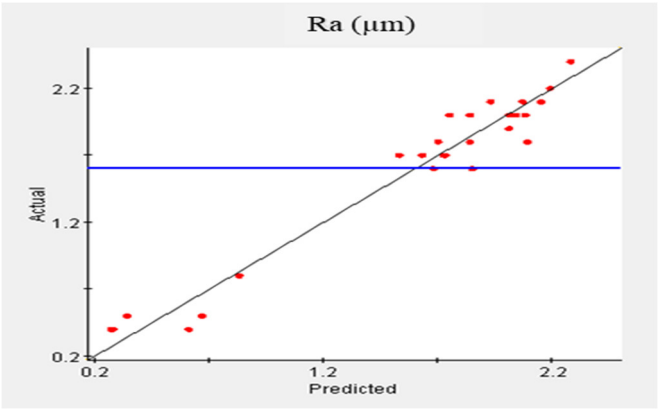

(b) $R^2 = 0.952$

Figure 7. The assessment of the RSM model: (a) for T and (b) for R_a using the coefficient of determination (R^2)

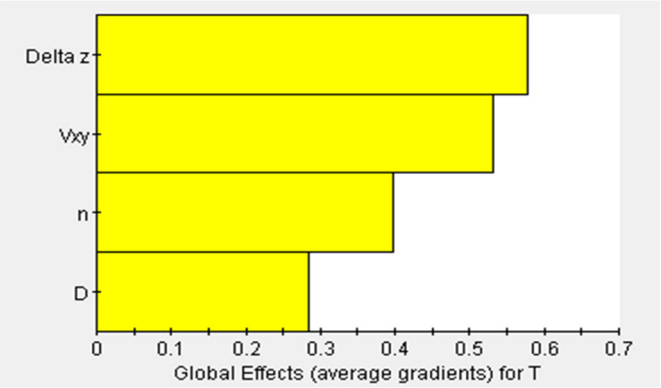

(a)

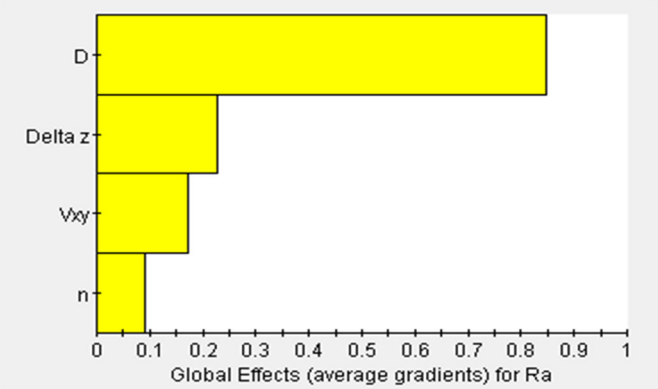

(b)

Figure 8. Global effects of investigated variables on (a) T and (b) R_a

The 3D surface plots are employed to visualize the simultaneous influence of two input variables on the output response, while keeping the remaining variables fixed at their median values. These plots aim to clarify the variation trends of the responses, reveal potential interaction effects between the parameters, and identify regions corresponding to optimal output values. Figures 9 and 10 illustrate the combined effects of two input factors on *T* and R_a, respectively. The response surfaces were constructed based on the regression models represented by Equations (1) and (2), where two factors were varied simultaneously and the others were held constant. All relevant response surfaces are comprehensively presented in Figures 9 and 10 to support the analysis of process behavior and optimization.

Figure 9a provides the relationship between *n* and V_{xy} regarding *T*, whereas Figure 9b explores the impact of *D* and *Δz*. Both demonstrate complex, interdependent relationships, suggesting optimal forming performance relies on the interplay between parameters rather than individual effects. In Figure 9a, *T* shows a significant decrease as *n* and V_{xy} increase from lower values, achieving a minimum around 800 - 1000mm/min and 1200 - 1400rpm, attributed to the increased efficiency of plastic deformation and enhanced material flow [12, 13]. *T* shows a slight increase outside these ranges, probably due to instability or surface defects resulting from an excessive deformation speed. Figure 9b illustrates that increasing *D* from 5 - 8mm to 12 - 14mm significantly reduces *T* due to improved stress distribution. A moderate *Δz* of 0.8 - 1.0mm also optimizes the deformation volume per pass. Nevertheless, a *Δz* exceeding 1.2mm results in stress concentration and geometric instability, undermining potential efficiency improvements [13].

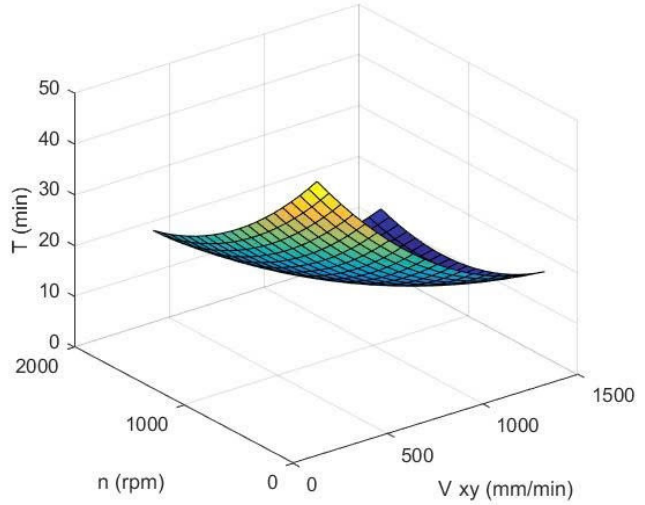

(a)

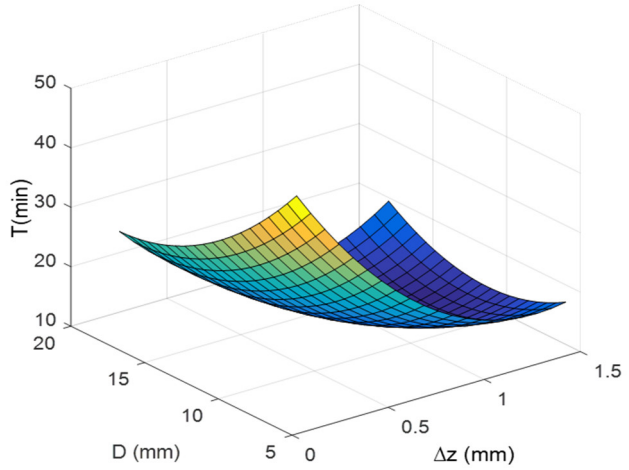

(b)

Figure 9. The 3D surface plots for T (other values are maintained at the middle level, respectively)

The response surfaces display saddle-like shapes, indicating that reducing forming time necessitates a balance between deformation volume and the continuity of material flow. Therefore, the ideal scenario integrates a balanced feed rate and rotation speed with an increased tool diameter and regulated vertical step, promoting efficiency, stability, and strong forming capabilities.

Figure 10 illustrates the critical role of synchronous parameter adjustment in reducing R_a during TPIF. In Figure 10a, R_a is lowest when the Δz is kept small and the D is limited to a relatively high level. Keeping Δz small reduces the deformation volume per pass, limiting stress gradients and notches. At the same time, a relatively high D ensures sufficient contact area without increasing the friction and waviness of the formed surface. This finding is consistent with recent incremental forming studies, which show that Δz and D are the primary factors affecting R_a, with small Δz and suitable D improving surface quality [11, 14].

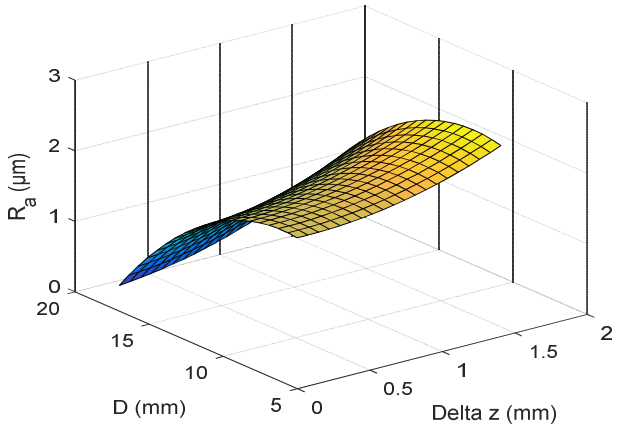

(a)

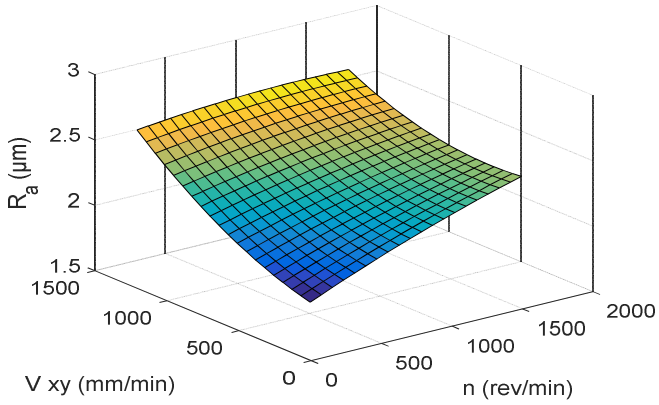

(b)

Figure 10. The 3D surface plots for R_a (other values are maintained at the middle level, respectively)

Figure 10b demonstrates the simultaneous impact of V_{xy} and speed n on R_a during TPIF. The figure reveals that R_a achieves its lowest value (~1.5 - 1.6μm) when both V_xy and n are at their lowest levels within the examined range. This can be explained by the fact that decreasing the feed rate and rotating speed helps to reduce the kinematic and thermal instabilities that commonly arise at high kinematic regimes [15]. Furthermore, when n is low, the relative sliding speed between the tool and the sheet metal is reduced, thereby minimizing frictional heat production and preventing surface softening, which can lead to local tearing or uneven material flow [1]. Similarly, V_{xy} reduces the feed rate between subsequent tool passes, lowering the trace's height on the surface and

generating a more level surface. Conversely, raising n or V_{xy} enhances the sharpness of the tool trace and may induce kinks due to varying speeds and non-uniform material flow [16]. This conclusion is consistent with prior incremental forming investigations, which have demonstrated that using a low kinematic parameter can give a superior surface finish in specific material and thickness combinations, due to reduced tool vibration, heat accumulation, and local strain concentration.

3.2. Multi-objective optimization using the NSGA-II

Based on the quadratic regression model of R_a and T, constructed using the RSM technique, which shows the relationship between the input variables and the resultant response in TPIF, the NSGA-II algorithm was applied to multi-objective optimization for T and R_a during the TPIF of A1050-H14. The optimization issue used four continuous input variables: tool ball diameter (D), vertical step size (Δz), feed rate in the XY plane (V_{xy}), and tool rotating speed (n), each confined within actual process bounds, as illustrated in Table 3.

Table 3. Input variables and constraint ranges for optimization

Input variables	Starting design point	Constraint ranges
Δz (mm)	0.8	$[0.1 < \Delta z < 1.5]$
V_{xy} (mm/min)	900	$[300 < V_{xy} < 1500]$
n (rpm)	1050	$[300 < n < 1800]$
D (mm)	12	$[6 < D < 18]$

Figure 11 illustrates the Pareto curve obtained by the combined method of RSM and NSGA-II, with many green and black points. The green points in Figure 11 represent the Pareto set, forming the Pareto curve, in which each point represents the optimal trade-off between the two objectives R_a and T. Conversely, the black points represent suboptimal solutions that do not effectively balance R_a and T. By representing specific Pareto points, it is possible to evaluate the influence of different levels of T on R_a, thereby determining the most effective operating parameters to optimize R_a and T through this trade-off simultaneously.

From Table 4 and Figure 11, they show the optimal parameter set for the input variables of the TPIF process of material A1050-H14, specifically including $\Delta z = 0.78$mm, $V_{xy} = 1136.75$mm/min, $n = 1576.88$rpm, and $D = 15.75$mm, corresponding to the achieved value of balance between the target $R_a = 1.13$µm and $T = 7.26$min. From these optimal values, the operator can directly input them into the GSK983M Milling CNC System to perform TPIF, as the system allows the entry of decimal values for V_{xy} and n. However, to simplify the setup process, these parameters may be rounded to the nearest integer values, namely $V_{xy} \approx 1137$mm/min and $n \approx 1577$rpm.

Table 4. Optimal results based on the NSGA-II

Input variables	Optimal results
Δz (mm)	0.78
V_{xy} (mm/min)	1136.75
n (rpm)	1576.88
D (mm)	15.75
T (min)	7.26
$R_a(\mu m)$	1.13

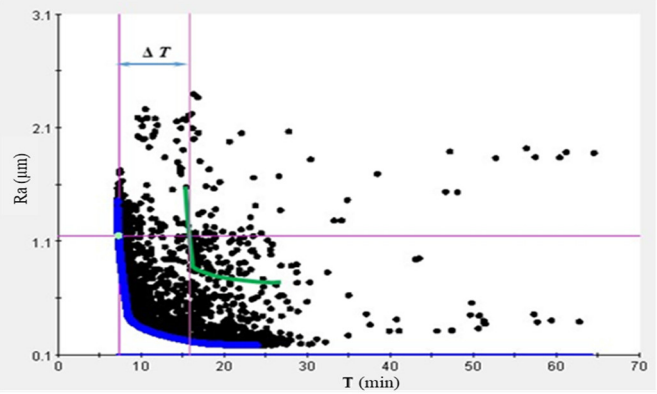

Figure 11. The Pareto plot for R_a and T based on the RSM model combined with NSGA-II

From the graph in Figure 11, it can be seen that, in the TPIF process, increased productivity, achieved by decreasing the forming time (T), is generally accompanied by a rise in surface roughness (R_a), indicating a decline in product quality after forming. On the contrary, if the purpose is to increase the surface quality, the machining time must be prolonged to achieve a superior surface finish. Therefore, based on the needs and real production circumstances, the operator can rely on this graph to select optimal operating settings, balancing productivity, surface quality, and production costs, thereby improving the process's economic and technical efficiency.

From Figure 11, imagine an arbitrary green curve is superimposed on the blue curve. If the operator sets a product quality target of $R_a = 1.3$µm and draws a horizontal line at this Ra level, the line will intersect the two curves at two distinct points. Two forming time values are obtained from these junction locations: $T_1 = 7.26$min and $T_2 = 16.05$min. The relative difference between these two numbers is derived using the formula: $\Delta T = (16.05 - 7.26) \times 100/16.05 = 54.77\%$.

This result reveals that picking the non-optimal point (T = 16.05min vs. T = 7.26min) increases the machining time by 54.77% without enhancing the surface quality. Applying RSM paired with NSGA-II enables the identification of more optimal solutions for R_a and T. For example, the difference in ΔT in Figure 11 highlights the value of selecting the optimal solution over any random solution. It confirms the usefulness of the RSM–NSGA-II approach in multi-objective optimization.

4. CONCLUSIONS

This work carefully explored the impacts of major process factors and multi-objective optimization on R_a and T in the TPIF of A1050 H14 material using the NSGA-II approach, which achieved the following outstanding results:

- The quadratic regression models for R_a and T based on the RSM in the TPIF of A1050-H14 material have been successfully created. The model's correctness has been tested using statistical analysis, which yields strong coefficients of determination for T and R_a, with R-squared values of 0.992 and 0.952, respectively. These values are close to 1. It can be inferred that the created model can predict the output responses of R_a and T during the TPIF process of A1050-H14 sheet material.

- The global effect study demonstrates that Δz is the parameter with the highest influence on T, while D is the factor with the most significant impact on R_a. This illustrates that in the TPIF process with A105-H14 material, if the aim is to increase machining productivity, attention should be given to changing Δz. At the same time, if the goal is to enhance surface quality, D plays a critical role.

- Successfully utilizing the NSGA-II approach, the best Pareto solution set was established, achieving a balance between R_a and T in the TPIF process of A1050-H14 material. The ideal parameter set achieved comprised Δz = 0.78mm, V_{xy} = 1137mm/min, n = 1577rpm, and D = 15.75mm, equivalent to R_a = 1.13µm and T = 7.26 minutes. This finding demonstrates that simultaneous optimization of two objectives can only be achieved by selecting a parameter set on the Pareto curve, thereby enhancing forming efficiency while maintaining good surface quality.

REFERENCES

[1]. M. Van Viet, N. T. Thinh, S. Antonov, "Study on the formability by TPIF technology for aluminium sheet at room temperature," *E3S Web of Conferences*, 207, 2020.

[2]. A. E. Ragab, "Multi-objective optimisation of profile accuracy in two point incremental forming using Taguchi-based grey relation analysis," *International Journal of Collaborative Enterprise,* 6, 1, 49-65, 2018.

[3]. M. V. Viet, *Study Forming for Metal Sheet by Two Point Incremental Forming (TPIF) Technology*. Doctoral Dissertation, Ho Chi Minh City University of Technology and Education, 2023.

[4]. S. Kopácsi, J. Nacsa, Á. Kisari, "Synchronized robot control for incremental sheet forming in the cyberspace," *Informatika-A Gábor Dénes Főiskola Közleményei,* 14, 2, 8-13, 2012.

[5]. R. J. Alves de Sousa, D. Afonso, F. Rubino, et al., "Potential of Incremental Forming Techniques for Aerospace Applications," *Materials, Structures and Manufacturing for Aircraft*, 293-315, 2022.

[6]. Y. Wu, "Application of aluminum alloy in aircraft," *Journal of Physics: Conference Series,* 2228(1), 012024, 2022.

[7]. H. Zhu, Y. Wang, J. Kang, "Research on combinatorial optimization of multidirectional sheet postures for forming thickness uniformity," *Journal of Mechanical Science and Technology,* 34, 10, 4251-4261, 2020.

[8]. Z. Liu, S. Liu, Y. Li, et al., "Modeling and optimization of surface roughness in incremental sheet forming using a multi-objective function," *Materials and Manufacturing Processes,* 29, 7, 808-818, 2014.

[9]. H. T. Nguyen, N. C. Vu, "Enhancing the Hard Turning Efficiency of 40Cr Alloy Steel with Coconut Oil-Based Nano-CuO Minimum Quantity Lubrication," *Mathematical Modelling of Engineering Problems,* 11, 12, 2024.

[10]. T. C. Hsiao, N. C. Vu, M. C. Tsai, et al., "Modeling and optimization of machining parameters in milling of INCONEL-800 super alloy considering energy, productivity, and quality using nanoparticle suspended lubrication," *Measurement and Control,* 54, 5-6, 880-894, 2021.

[11]. T. V. Nguyen, T. Vo, N. T. Phan, et al., "Reviews on the Effect of Single Point Incremental Forming (SPIF) Process Parameters on Surface Roughness of Aluminum Alloy AA1050-H14 Sheet Metal," *Applied Mechanics and Materials,* 914, 151-162, 2023.

[12]. P. Verleysen, J. Peirs, L. Duchene, "Determination of the high strain rate forming properties of steel sheet," *COMPLAS XI: proceedings of the XI International Conference on Computational Plasticity: Fundamentals and Applications*. CIMNE, 2011.

[13]. R. Diefenderfer, C. Vanderwiel, I. Ragai, et al., "Influence of Tool Diameter in Single Point Incremental Forming of Polymeric Materials," *ASME International Mechanical Engineering Congress and Exposition*, 88605, 2024.

[14]. M. Szpunar, R. Ostrowski, A. Dzierwa, "Effect of single-point incremental forming process parameters on roughness of the outer surface of conical drawpieces from cp titanium sheets," *Advances in Mechanical and Materials Engineering,* 41, 1, 221-231, 2024.

[15]. M. Van Viet, N. T. Thinh, L. V. Sy, "Influence of machining parameters on the TPIF formability for aluminum sheet at room temperature," in *International Conference on Material, Machines and Methods for Sustainable Development*. Cham: Springer International Publishing, 238-245, 2020.

[16]. H. Y. Maan, W. Hamdan, "Determining the effect of process parameters on surface roughness in two point incremental sheet metal forming process using the Taguchi method," *Engineering and Technology Journal,* 33, A-7, 1569-1582, 2015.